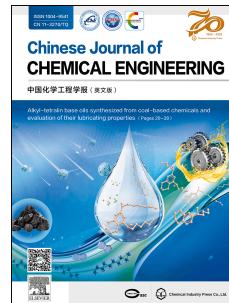


# Journal Pre-proof

Graphene oxide framework membranes intercalated by poly(sodium 4-styrenesulfonate) for efficient desalination

Hui Xu, Jincheng Huang, Hong Qi



PII: S1004-9541(25)00350-7

DOI: <https://doi.org/10.1016/j.cjche.2025.06.036>

Reference: CJCHE 3676

To appear in: *Chinese Journal of Chemical Engineering*

Received Date: 2 March 2025

Revised Date: 22 April 2025

Accepted Date: 6 June 2025

Please cite this article as: H. Xu, J. Huang, H. Qi, Graphene oxide framework membranes intercalated by poly(sodium 4-styrenesulfonate) for efficient desalination, *Chinese Journal of Chemical Engineering*, <https://doi.org/10.1016/j.cjche.2025.06.036>.

This is a PDF file of an article that has undergone enhancements after acceptance, such as the addition of a cover page and metadata, and formatting for readability, but it is not yet the definitive version of record. This version will undergo additional copyediting, typesetting and review before it is published in its final form, but we are providing this version to give early visibility of the article. Please note that, during the production process, errors may be discovered which could affect the content, and all legal disclaimers that apply to the journal pertain.

© 2025

Type of the study: Original research article

**Graphene oxide framework membranes intercalated by  
poly(sodium 4-styrenesulfonate) for efficient desalination**

Hui Xu<sup>1</sup>, Jincheng Huang<sup>1</sup>, Hong Qi<sup>1</sup> \*

<sup>1</sup> College of Chemical Engineering, Nanjing Tech University, Nanjing 210009, China

Version date: 2025.03.02

Corresponding author: Hong Qi (Ph.D., Full Professor)

Tel. +86-25-83172279

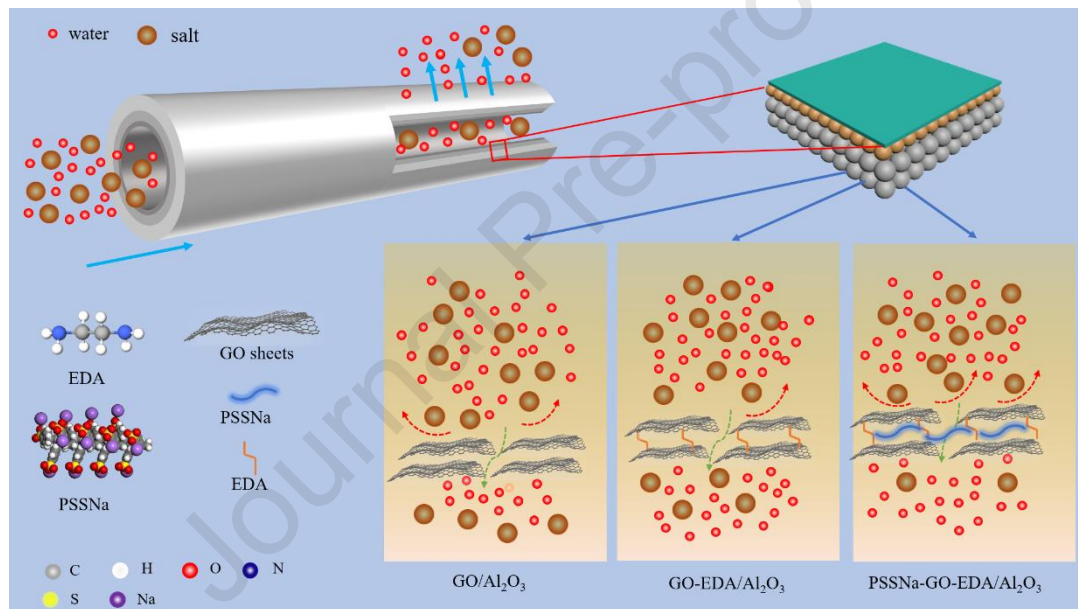
Email: hqi@njtech.edu.cn

# Graphene oxide framework membranes intercalated by poly(sodium 4-styrenesulfonate) for efficient desalination

Hui Xu, Jincheng Huang, Hong Qi \*

College of Chemical Engineering, Nanjing Tech University, Nanjing 210009, China

\* Tel. +86-25-83172279; Email: [hqi@njtech.edu.cn](mailto:hqi@njtech.edu.cn)



1                   **Graphene oxide framework membranes intercalated by**  
2                   **poly(sodium 4-styrenesulfonate) for efficient desalination**

3                   Hui Xu, Jincheng Huang, Hong Qi \*

4                   College of Chemical Engineering, Nanjing Tech University, Nanjing 210009, China

5                   \* Email: hqi@njtech.edu.cn

6                   **Abstract**

7                   GO membranes with well-defined sub-nanometer channels are optimal for desalination  
8                   and wastewater purification. However, the inherent instability of the interlayer structure  
9                   and the severe trade-off between selectivity and permeability pose a significant  
10                  challenge for GO membranes to be effectively applied to nanofiltration. Herein, we  
11                  synthesized a series of PSSNa-GO-EDA/Al<sub>2</sub>O<sub>3</sub> membranes by embedding poly(sodium  
12                  4-styrenesulfonate) (PSSNa) into ethylenediamine-crosslinked GO interlayers. The  
13                  resultant membranes exhibited greater interlayer structures, in which new hydrophilic  
14                  confined nanostructures were constructed. Effective nanofiltration performance was  
15                  achieved through electrostatic-induced ion-confined partitioning. The PSSNa-GO-  
16                  EDA-1/Al<sub>2</sub>O<sub>3</sub> (**PGE-1**) membrane showed high rejection rates of 86.0% for Na<sub>2</sub>SO<sub>4</sub>  
17                  and 53.8% for NaCl while maintaining competitive pure water permeance of 10.85  
18                  LMH/bar, which is 12.1 times higher than that of the pristine GO membrane. More  
19                  importantly, after immersion in pure water for 680 hours, this membrane retained  
20                  commendable separation performance. Overall, our work provides an effective strategy  
21                  to finely fabricate confined nanostructures in lamellar GO-based nanofiltration  
22                  membranes featuring excellent separation performance.

23                  **Keywords:** Graphene oxide membrane; PSSNa; Confined nanostructures; Desalination

1    **1. Introduction**

2       Owing to accelerated industrialization, population expansion, and freshwater  
3    pollution, the scarcity of clean water has emerged as one of the greatest humanitarian  
4    crises worldwide[1, 2]. To solve the issue of water scarcity, a range of separation and  
5    purification technologies have been developed. In contrast to traditional purification  
6    techniques such as distillation and electrodialysis, membrane separation technology has  
7    demonstrated excellent application prospects due to its benefits of lower energy  
8    consumption, higher efficiency, and eco-friendliness [3-5].

9       Graphene oxide, a kind of novel two-dimensional material, has drawn significant  
10   attention due to its atomic thickness, outstanding physicochemical properties, and  
11   easily functionalized surface characteristics[6-9]. Additionally, self-supported GO  
12   membranes could be directly synthesized through the stacking of GO nanosheets[10].  
13   Nevertheless, the self-supported GO membrane faces numerous difficulties in practical  
14   applications. Simultaneously, on account of its swelling property, it is difficult for the  
15   GO membrane to ensure the stability of the laminar structure in water [11, 12]. Even  
16   more seriously, the laminar GO membranes possess tortuous, narrow, and lengthy  
17   transport channels, which have high solute rejection rates but are often accompanied by  
18   extremely low water permeability. This situation severely restricts the application of  
19   GO membranes due to the selectivity-permeability trade-off[13, 14].

20       In response to the challenges in the applications of GO membranes, numerous  
21   methods have been developed over the past two decades[15, 16], such as physical  
22   confinement, thermal or chemical reduction, and cross-linking. For example, Abraham  
23   *et al.* [17] achieved the adjustment of the interlayer distance of laminar GO membranes  
24   from 9.8 Å to 6.4 Å by employing epoxy resin for encapsulation. On the other hand, an  
25   extensive array of crosslinkers with diverse chemical properties and functionalities has  
26   been extensively employed to overcome the swelling of GO membranes. Molecules or  
27   polymers containing amine groups are regarded as ideal crosslinkers for GO  
28   membranes, such as polydopamine [18], polyethyleneimine [19], amino acids[20],

1 ginger plant extractive [21], and ethylenediamine [22]. For instance, Jin *et al.* [23] put  
2 forward a method of constructing "molecular bridges" which they rationally built and  
3 tuned to stabilize the GO membranes. The molecular-bridged GO membranes  
4 demonstrated exceptional durability under severe operating conditions. Consequently,  
5 the molecular-bridged GO membranes had an outstanding dye removal rate of over  
6 99%. Its ion rejection, however, was not satisfactory.

7 Naturally, the covalent or non-covalent cross-linking method is not limited to the  
8 application of a single cross-linker but is also widely employed for double cross-linkers  
9 [24, 25]. For example, Xu *et al.* [26] used metal-polyphenol double-crosslinked GO  
10 membranes for dye/salt separation. Their results indicated that the membrane not only  
11 showed a larger interlayer spacing and superior hydrophilicity, but its surface negative  
12 charge also exhibited a decreasing tendency. Hence, the membranes exhibited an  
13 exceptional removal rate for organic dyes, reaching 99% or more, and a high  
14 permeability of 61.2 LMH per bar.

15 For two-dimensional laminar GO membranes, regulating the interlayer distance  
16 and modifying the surface chemical characteristics or interlayer can be effective ways  
17 to achieve excellent separation performance. Shao *et al.* [27] designed a novel  
18 coordination complex as the modifier to fabricate hydrophilic GO membranes. The  
19 interaction between the  $\text{Fe}^{3+}$ -phytic acid coordination complex and the GO nanosheets  
20 modulated the interlayer distance of the GO membranes. As a result, this complex  
21 enhanced the hydrophilic characteristics of GO membrane surfaces, improved the  
22 composite membrane's water sorption capacity and facilitated rapid water transport.  
23 Moreover, Dai *et al.* [28] stabilized the stacked laminar GO membrane structure by  
24 introducing sodium polystyrene sulfonate into the interlayer of the GO membrane. Due  
25 to the exceptional properties of the sulfonic acid groups, the modified structure is both  
26 hydrophilic and charged in the interlayer structure, providing a favorable hydrophilic  
27 microenvironment to facilitate selective water molecule transport. Their results  
28 revealed that the PSSNa/GO membrane fabricated with this strategy demonstrates

1 exceptional pervaporation separation properties.

2 Therefore, the enhancement of the stability of the laminar structure of GO  
3 membranes, coupled with the establishment of chemically distinct environments or  
4 microregions with specialized confinement functions on the surface or within the  
5 interlayers, represents a pivotal strategy for optimizing the performance of lamellar GO  
6 membranes in water.

7 In this paper, we incorporated sodium polystyrene sulfonate into the amine-  
8 crosslinked GO membrane interlayer and deposited GO-based nanosheets onto the  
9 inner tube ceramic membranes via the pressure-assisted deposition approach. The  
10 resultant GO composite ceramic nanofiltration membranes were prepared as depicted  
11 in Fig. 1. We have developed a new approach to creating hydrophilic confined  
12 nanostructures within the interlayer of GO membranes. This method has the potential  
13 to stabilize the laminar structures of these membranes and increase interlayer spacing,  
14 which could enhance pure water permeability. Additionally, it may be effective in  
15 confining ions in saline solutions via ion electrostatic induction forces. This mechanism  
16 significantly mitigates the synergistic transport effects between cations and anions,  
17 thereby improving rejection rates. The results demonstrate that the PSSNa-GO-EDA-  
18 1/Al<sub>2</sub>O<sub>3</sub> (PGE-1) membrane achieves rejection rates of 86.0% for Na<sub>2</sub>SO<sub>4</sub> and 56.4%  
19 for NaCl while maintaining competitive water permeability of 10.85 LMH per bar  
20 (12.1-fold higher than that of pristine GO membrane). Moreover, the PSSNa-GO-EDA-  
21 1/Al<sub>2</sub>O<sub>3</sub> membrane demonstrates outstanding stability during long-term filtration  
22 processes. Thus, we are confident that this approach will significantly enhance practical  
23 applications of GO membranes in water purification.

24 **2. Experimental**

25 **2.1. Materials**

26 GO nanosheets (lateral size: 500–5000 nm, 1 mg·ml<sup>-1</sup>, XFNANO), Tris  
27 (hydroxymethyl) aminomethane hydrochloride (Tris-HCl, 99%, Aladdin),

1 Hydrochloric acid (HCl, 36% (mass), Lingfeng), poly(sodium 4-styrenesulfonate)  
 2 (PSSNa, MW=70000, 99%, Aladdin), Anhydrous ethylenediamine (EDA, 99%,  
 3 Adamas), Na<sub>2</sub>SO<sub>4</sub>, NaCl, MgSO<sub>4</sub>, and MgCl<sub>2</sub> (99%, Lingfeng), Dopamine  
 4 hydrochloride (98%, Aladdin) were used without additional purification. 110-mm-long  
 5 tubular Al<sub>2</sub>O<sub>3</sub> ceramic membranes with inner and outer diameters of 8 and 12 mm (pore  
 6 size: 20 nm) were obtained from Hongyi (Nanjing, China).

7 **2.2 Preparation of PDA- pre-treated tubular Al<sub>2</sub>O<sub>3</sub> ceramic membranes**

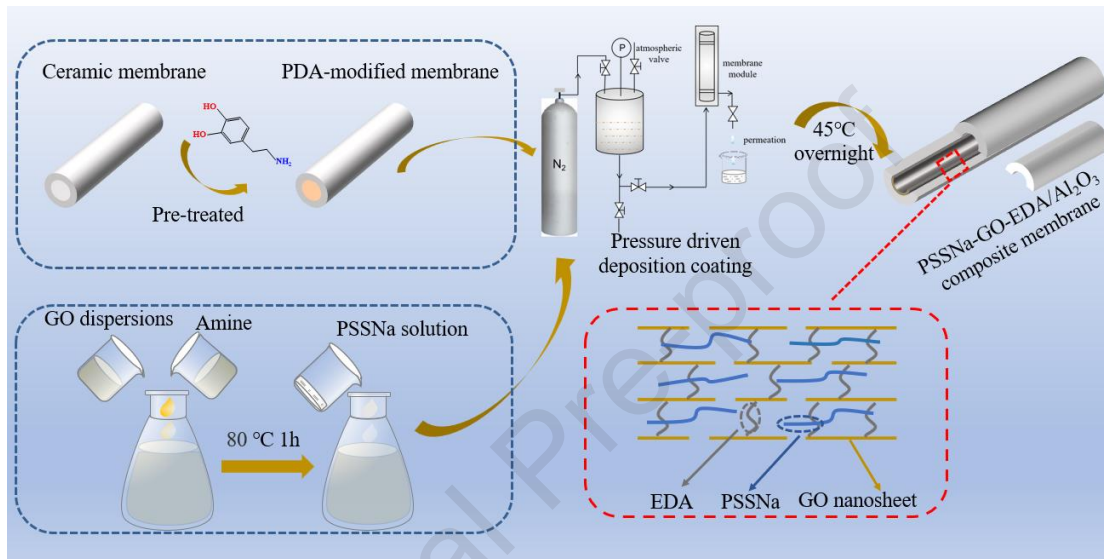
8 First of all, 2 mg/ml aqueous solution of dopamine hydrochloride was mixed with  
 9 10 mM Tris-HCl solution stirring at 25 °C. After thoroughly mixing the solution, the  
 10 tubular Al<sub>2</sub>O<sub>3</sub> membranes were subsequently treated with this solution at 25 °C for 20  
 11 hours to promote the self-polymerization of polydopamine in a dark environment.  
 12 Following this, the membranes were rinsed with pure water to remove any residual  
 13 dopamine from the inner surface of the tubular Al<sub>2</sub>O<sub>3</sub> membranes. Finally, the tubular  
 14 ceramic membranes were dried in an electric-heated constant-temperature air-  
 15 circulating drying oven at 60 °C for two hours to obtain polydopamine-modified Al<sub>2</sub>O<sub>3</sub>  
 16 membranes, hereafter referred to as the PDA-Al<sub>2</sub>O<sub>3</sub> membranes.

17 **2.3 Preparation of pristine GO and GO-based membranes**

18 First, 0.2 ml of GO dispersion was diluted to 200 ml with pure water, and the  
 19 single-layer GO nanosheets were completely dispersed in the 200 ml dilution by  
 20 sonication for 10 min. After that, to prepare the GO-EDA (GE) suspension, 13.5 µl of  
 21 EDA was added to the GO solution. After thoroughly mixing the solution, the mixture  
 22 was stirred at 80 °C for 60 min. Subsequently, the prepared GE suspension was mixed  
 23 with a specific quantity of sodium polystyrene sulfonate aqueous solution and sonicated  
 24 for 15 minutes to form a homogeneous PSSNa-GO-EDA (PGE)solution.

25 The suspensions with different amounts of PSSNa were loaded onto the internal  
 26 surface of the prepared PDA-Al<sub>2</sub>O<sub>3</sub> membrane under pressurized nitrogen at 1 bar.  
 27 Finally, the fabricated membranes were dried at 45 °C overnight in an electric-heated  
 28 constant-temperature air-circulating drying oven to obtain PSSNa-GO-EDA/Al<sub>2</sub>O<sub>3</sub>

1 membranes. The resulting PSSNa-GO-EDA/Al<sub>2</sub>O<sub>3</sub> membranes were labeled PGE-*x* (*x*  
 2 = 1, 2, 3). The theoretical mass ratios of GO and PSSNa are 1:150, 1:250, and 1:400,  
 3 and the composite membranes are named PGE-1, PGE-2, and PGE-3, respectively.  
 4 Pristine GO and GO-EDA membranes were fabricated following the same strategy,  
 5 except that EDA and PSSNa were not added. The preparation process of the PGE  
 6 membranes is illustrated in Fig. 1.



7 **Fig. 1.** Schematic diagram of the preparation processes of PGE membranes

8 **2.4 Characterizations of GO and GO-based membranes**

9 Zeta potential of the prepared membrane samples was tested by Zetasizer analyzer  
 10 (Nano ZS-90). Fourier transform infrared spectrometer (FT-IR, Nicolet 8700), X-ray  
 11 photoelectron spectroscopy (XPS, Al K $\alpha$ , ESCALAB 250), X-ray diffraction (XRD,  
 12 Cu K $\alpha$ , Mini Flex 600), and Scanning electron microscopy (SEM, Sigma 360) were  
 13 performed to investigate the chemical composition, the interlayer structure and the  
 14 morphologies of the prepared membrane samples, respectively. The contact angles (CA)  
 15 of the prepared membrane samples were measured using a contact angle tester (Drop  
 16 Meter A-100P).

17 **2.5 Evaluation of the membrane performance**

18 The prepared membrane separation performance was evaluated using 1 mmol·L<sup>-1</sup>  
 19 single-component salt solutions (Na<sub>2</sub>SO<sub>4</sub>, MgSO<sub>4</sub>, NaCl, MgCl<sub>2</sub>) under 5 bar on a self-  
 20

1 built cross-flow filtration device at 25 °C. The stability of the GO-based membranes  
 2 was tested through a long-term water immersion test. The pure water permeance of GO-  
 3 based membranes were tested continuously for 4 h. The salt rejection performance test  
 4 was conducted after the system was stabilized for 40 minutes. Subsequently, to ensure  
 5 data accuracy, the permeate was collected at 5-minute intervals for a total of four  
 6 collections.

7 After soaking the GO-based membranes in pure water for different periods of time  
 8 (170, 340, 510 and 680 h), the rejection of the above four single-component salt  
 9 solutions was measured under the corresponding soaking time. The pure water  
 10 permeance  $J$  (LMH/bar) and the salt rejection  $R$  are calculated with the following  
 11 equations:

$$12 \quad J = \frac{V}{At\Delta P} \quad (1)$$

$$13 \quad R = (1 - \frac{C_p}{C_f}) \times 100\% \quad (2)$$

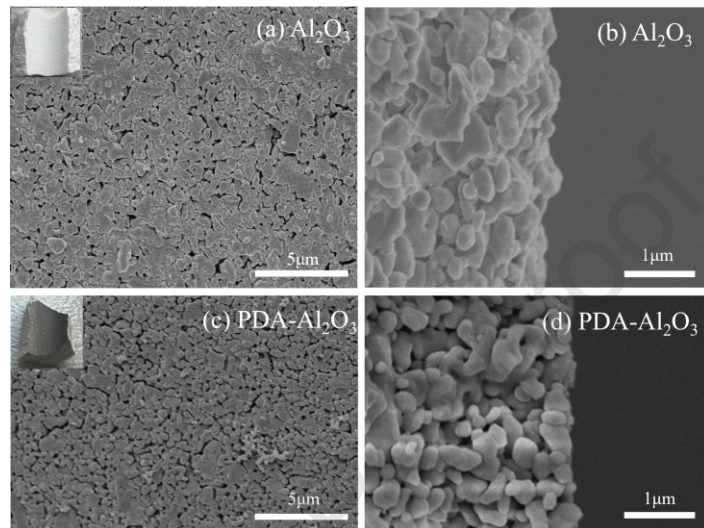
14 where  $V$  (L) is the volume of permeate;  $A$  ( $m^2$ ) is the effective membrane area;  $t$  (h) is  
 15 permeation time;  $\Delta P$  (bar) is the operating pressure.  $C_f$  and  $C_p$  are the feed and  
 16 permeate concentrations of salt solutions.

### 17 3. Results and discussion

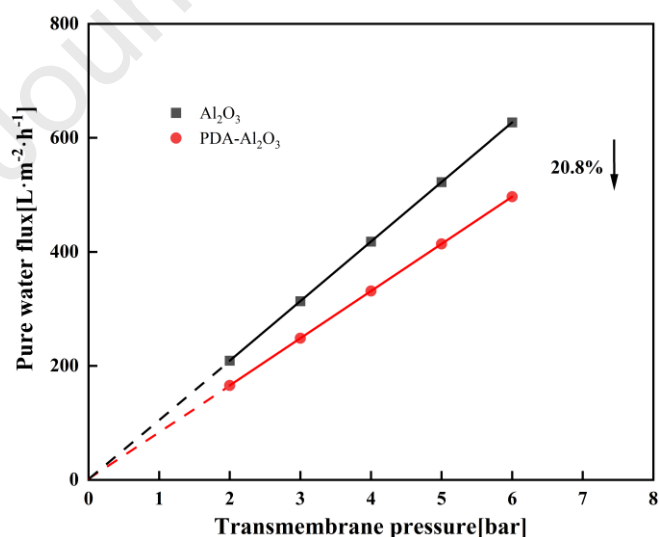
#### 18 3.1 Performance of the PDA-Al<sub>2</sub>O<sub>3</sub> tubular membrane

19 The morphologies of Al<sub>2</sub>O<sub>3</sub> and PDA-Al<sub>2</sub>O<sub>3</sub> membranes were analyzed using SEM.  
 20 As shown in Fig. 2, the alumina particles are evenly dispersed on the surface of the  
 21 Al<sub>2</sub>O<sub>3</sub> membrane, and the surface of PDA-Al<sub>2</sub>O<sub>3</sub> membrane is obviously covered with  
 22 a material layer. It is also evident from the optical images that the membrane surface  
 23 turns black following PDA modification. From Fig. 2(b), (d), the PDA is closely  
 24 covered on the Al<sub>2</sub>O<sub>3</sub> membrane without obvious boundary. The pure water flux of the  
 25 Al<sub>2</sub>O<sub>3</sub> and PDA-Al<sub>2</sub>O<sub>3</sub> membranes was evaluated. It can be seen from Fig. 3 that the  
 26 modified membrane exhibits a 20.8% reduction in pure water permeance (82.8

1 LMH/bar) compared with that before modification. Furthermore, the rejection rates of  
 2 the  $\text{Al}_2\text{O}_3$  and PDA- $\text{Al}_2\text{O}_3$  membranes for the four salt solutions are all below the  
 3 detection limit of the conductivity meter (the rejection rates can be regarded as zero).  
 4 The results indicate that PDA was successfully grafted on the  $\text{Al}_2\text{O}_3$  membrane via self-  
 5 polymerization [29].



7 **Fig. 2.** SEM images of (a, c) surfaces, (b, d) cross-sections of the  $\text{Al}_2\text{O}_3$  and PDA-  
 8  $\text{Al}_2\text{O}_3$  membranes

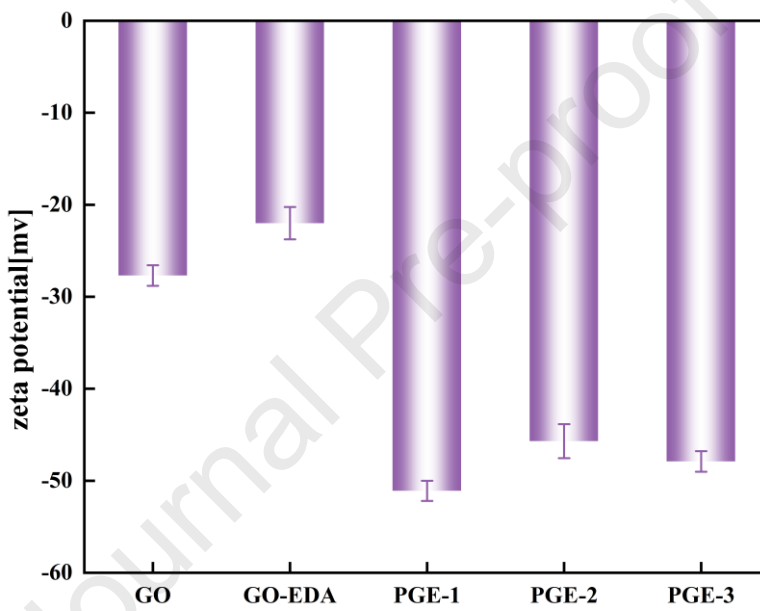


10 **Fig. 3.** Pure water flux of  $\text{Al}_2\text{O}_3$  and PDA- $\text{Al}_2\text{O}_3$  tubular membranes

### 11 3.2 Characterizations of GO-based membranes

12 The well-dispersible GO suspension constitutes a prerequisite for preparing

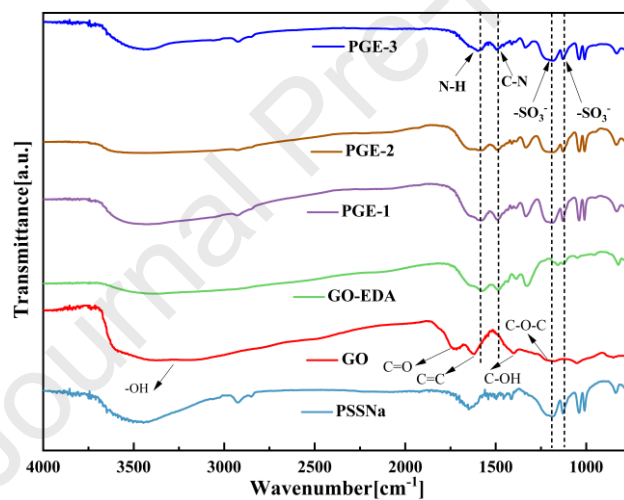
1 separation membranes with excellent performance. As shown in Fig. 4, the zeta  
 2 potential of the five membrane-forming suspensions is all negative, and the lowest zeta  
 3 potential is witnessed in the PGE-1. This is attributed to the abundant negatively  
 4 charged ionized sulfonic acid groups in PSSNa, which gives rise to a reduction in the  
 5 zeta potential of the suspensions containing PSSNa. The lower the zeta potential is, the  
 6 better the dispersibility of the suspension becomes. This is conducive to depositing  
 7 nanosheets on the tubular ceramic membrane in preparing GO-based separation  
 8 membranes with good laminar structure.



9  
 10 **Fig. 4.** Zeta potential of pristine GO, GE, PGE membrane-forming suspension

11 Fig. 5 shows the FTIR spectra of PSSNa, pristine GO, GE, and PGE membranes;  
 12 the characteristic peaks of the pristine GO membrane located at  $\sim 3443$ ,  $\sim 1729$ ,  $\sim 1625$ ,  
 13  $\sim 1406$ , and  $\sim 1226\text{ cm}^{-1}$  were assigned to  $-\text{OH}$ ,  $\text{C}=\text{O}$ ,  $\text{C}=\text{C}$ ,  $\text{C}-\text{OH}$ , and  $\text{C}-\text{O}-$   
 14  $\text{C}$ , respectively. These values are in agreement with the previous report [30]. When the  
 15 GO nanosheets were crosslinked with EDA, the characteristic peaks of carboxyl and  
 16 epoxy groups were no longer observed due to the existence of EDA [31]. Besides, there  
 17 are two peaks at  $\sim 1583$  and  $\sim 1481\text{ cm}^{-1}$ , which can be attributed to amine ( $\text{N}-\text{H}$ ) and  
 18 amide ( $\text{C}-\text{N}$ ) respectively [32]. This occurs due to the covalent reaction of the amine  
 19 groups in EDA with the oxygenated groups on the GO laminar nanosheets[33], thus  
 20 proving the successful introduction of EDA into the GO membranes. For PGE

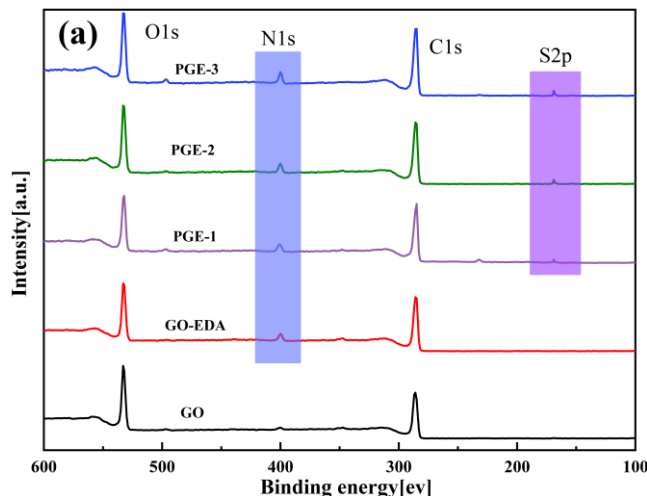
1 membranes, there are two additional distinct peaks located at  $\sim 1129$  and  $\sim 1191$   $\text{cm}^{-1}$   
 2 [28]. These peaks indicate the stretching vibration of  $\text{S}=\text{O}$  of  $-\text{SO}_3^-$ , which  
 3 substantiates the incorporation of PSSNa into the two-dimensional interlayer channel  
 4 of GO-based membranes. Furthermore, the XPS full-spectrum in Fig. 6 shows that the  
 5 novel peaks at 400 eV were identified in both GE and PGE membranes, corresponding  
 6 to the N 1s convolution peak [31]. Meanwhile, new peaks at 168 eV were detected in  
 7 the PGE membranes. Further fitting of the S 2p curve reveals that the two additional  
 8 distinct peaks at 167.8 eV and 169.0 eV represent the oxidized sulfur in the  $-\text{SO}_3^-$ ,  
 9 which was attached to the benzene structure within PSSNa [28, 34]. These findings  
 10 demonstrate that EDA and PSSNa have effectively introduced two-dimensional  
 11 interlayer channels into GO membranes.



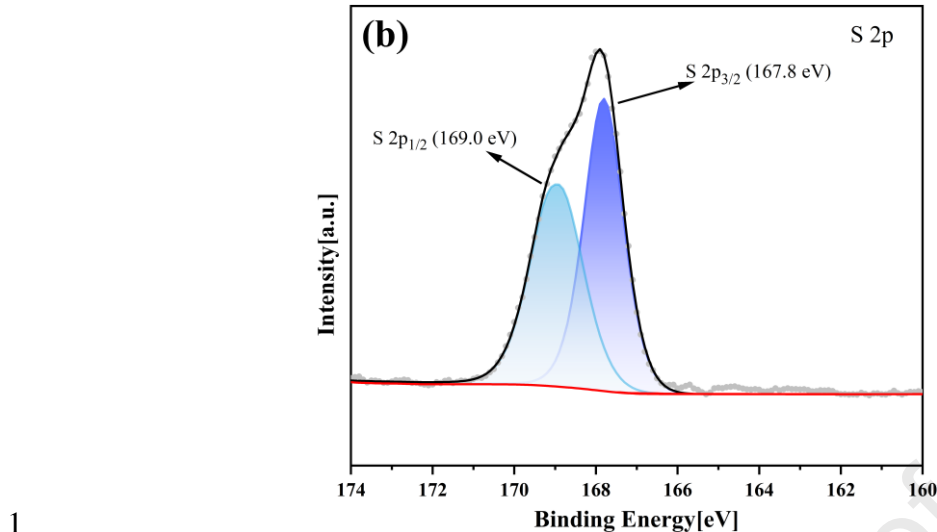
12 **Fig. 5.** FTIR spectra of PSSNa, GO, GE, and PGE membranes

13

14

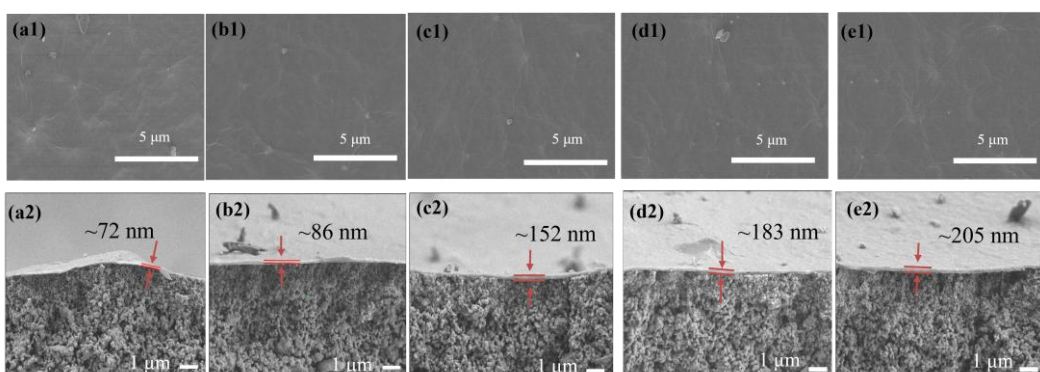


15



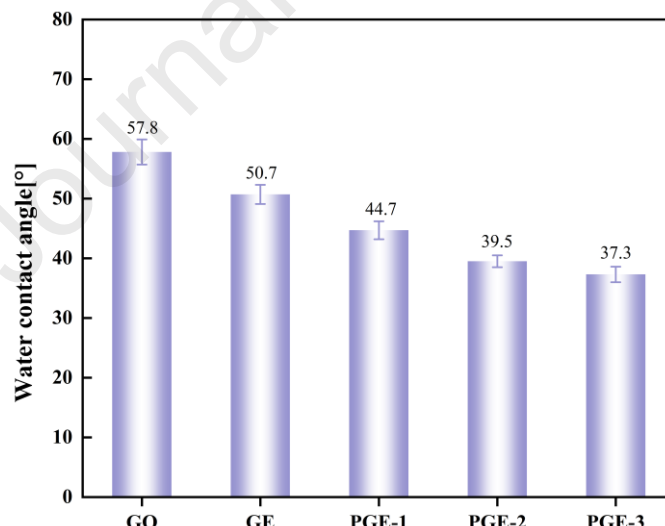
2 **Fig. 6.** (a) XPS full-scan spectra of GO, GE, and PGE membranes; (b) S 2p  
 3 spectra of PGE-1 membrane

4 For lamellar separation membranes, a complete and defect-free membrane  
 5 structure is of crucial significance for their application. As shown in Fig. 7, the surfaces  
 6 of the GO, GE, and PGE membranes are smooth and continuous, and all of them  
 7 possess typical wrinkles, suggesting that the GO-based membranes have been  
 8 successfully coated onto the tubular ceramic support. Furthermore, the thickness of the  
 9 pristine GO membrane layer was 72 nm according to Fig. 7(a2), while those of the GE,  
 10 PGE-1, PGE-2, and PGE-3 membranes increased to 86, 152, 183, and 205 nm,  
 11 respectively, with the intercalation of EDA and PSSNa into the interlayer structure.  
 12 Additionally, all five membranes maintain excellent interlayer structures.



13 **Fig. 7.** SEM images of (a1) GO, (b1) GE, (c1) PGE-1, (d1) PGE-2, (e1) PGE-3  
 14 membrane surfaces and (a2) GO, (b2) GE, (c2) PGE-1, (d2) PGE-2, (e2) PGE-3  
 15  
 16 membrane cross-sections

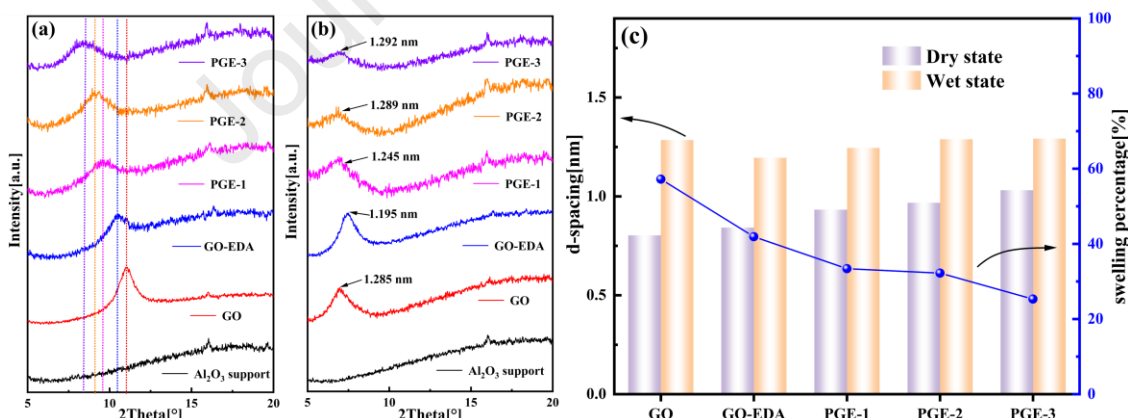
1        Normally, water molecules exposed to the membrane surface will be absorbed into  
 2        the membrane by the chemical potential difference [35, 36]. Consequently, as the  
 3        membrane layer becomes more hydrophilic, water molecules are able to penetrate the  
 4        membrane more readily. Therefore, to evaluate the hydrophilicity of the membrane, we  
 5        measured the water contact angle (WCA) of the GO, GE, and PGE membranes. As  
 6        illustrated in Fig. 8, the WCA of the pristine GO membrane is  $57.8^\circ$ ; this finding is in  
 7        agreement with the results presented in the prior study [33] and indicates that the  
 8        membrane is of a hydrophilic nature. With the crosslinking of EDA, the WCA of the  
 9        GE membrane reduced, as the diamine groups crosslinked on the GE membrane layer  
 10       are hydrophilic and prone to forming hydrophilic regions. This effect could enhance the  
 11       hydrophilicity of the GE membrane layer [32, 33]. For the PGE-1, PGE-2, and PGE-3  
 12       membrane, the WCA decreased from  $44.7^\circ$  to  $37.3^\circ$ . PSSNa contains a significant  
 13       number of hydrophilic sulfonic acid groups, and incorporating PSSNa into lamellar GO  
 14       membranes can enhance the ability of PGE membranes to attract water molecules.



15  
 16       **Fig. 8.** WCA of GO, GE, and PGE membranes

17       The laminar interlayer structures of the GO, GE, and PGE membranes were  
 18       analyzed by XRD. Fig. 9 presents the XRD patterns of GO, GE, and PGE membranes.  
 19       There is a diffraction peak at  $11.02^\circ$  for the pristine GO membrane, corresponding to  
 20       an interlayer spacing of 0.803 nm. This is consistent with the Ref. [37]. For the GE  
 21       membrane, the diffraction peak shifts to a lower angle ( $2\theta=10.50^\circ$ ), indicating an

1 expanded interlayer spacing of 0.842 nm. This phenomenon can be attributed to the  
 2 incorporation of EDA molecules, which induces an expansion of the interlayer spacing  
 3 in the GO membrane. In comparison with the pristine GO and GE membranes, with the  
 4 increase of PSSNa crosslinking amount, the diffraction peaks of the PGE-1, PGE-2,  
 5 and PGE-3 membranes shift to even lower angles ( $2\theta=9.48^\circ$ ,  $9.14^\circ$ , and  $8.58^\circ$ ,  
 6 respectively), corresponding to interlayer spacings of 0.933, 0.968 and 1.031 nm,  
 7 respectively. These findings indicate a further expansion of the interlayer spacing in the  
 8 GO membrane, which facilitates reduced mass transfer resistance and significantly  
 9 enhances water permeability. Furthermore, we performed XRD measurements on GO-  
 10 based membranes in their wet states and systematically compared the variations in  
 11 interlayer spacing between the dry and wet conditions. The results demonstrate that the  
 12 swelling ratio of the interlayer spacing for the pristine GO membrane in the wet state is  
 13 57.2%. After EDA intercalation, the swelling ratio decreases to 41.9%. With the  
 14 addition of PSSNa, the swelling behavior of the GO membrane is further limited.  
 15 Collectively, these results suggest that the interlayer structural stability of the GO  
 16 membrane is significantly improved under the synergistic effects of EDA and PSSNa.



17 **Fig. 9.** XRD patterns of the GO-based membranes in the (a) dry and (b) wet states; (c)  
 18 d-spacing and swelling percentage of GO-based membranes in dry and wet conditions  
 19

### 20 3.3 Pure water permeability of GO-based membranes

21 The pure water permeance of GO, GE, PGE-1, PGE-2, and PGE-3 was tested  
 22 continuously for 4 h a custom-built cross-flow filtration device, and the results are

1 shown in Fig. 10. As the operation time increased, the permeation of GO, GE, PGE-1,  
2 PGE-2, PGE-3 membrane initially decreased before stabilizing. Pure water permeance  
3 in a stable state of GO, GE, PGE-1, PGE-2, and PGE-3 was 0.90, 1.46, 10.85, 4.59, and  
4 4.12 LMH/bar. This result can be explained by the relatively loose structure and  
5 incomplete stacking of the GO nanosheets at the initial stage of filtration, which creates  
6 wide transport channels that facilitate the flow of water molecules [38]. However, as  
7 cross-flow time increases, the pressure gradually compresses this loose microstructure,  
8 reducing the available water transport pathways and decreasing permeance. The  
9 permeance of the GE membrane was found to be higher than that of the pristine GO  
10 membrane. This can be attributed to the increased interlayer distance resulting from the  
11 addition of EDA. Compared with pristine GO membrane, it can also be found that the  
12 permeability of PGE membranes (PGE-1, PGE-2, and PGE-3) was increased by 12.1,  
13 5.1, and 4.6 times, respectively. The improvement in permeance can be attributed to the  
14 increase in interlayer distance of the PGE membranes caused by the introduction of  
15 EDA and PSSNa. Furthermore, the hydrophilic sulfonic acid groups, crosslinked within  
16 the interlayer of PGE membranes, could capture water molecules more effectively, thus  
17 creating additional pathways for water molecule transport. Consequently, the  
18 permeance of PGE membranes was greatly improved. The permeability of the PGE-1  
19 membrane is higher than that of PGE-2 and PGE-3 membrane, which may be due to  
20 the following reasons. First, the thickness of PGE-2 and PGE-3 membrane increases,  
21 resulting in an increased mass transfer path and higher resistance for water molecules.  
22 Second, the excessive insertion of PSSNa could expand the interlayer spacing positively.  
23 Meanwhile, it also occupies a large amount of interlayer space to some extent,  
24 subsequently leading to a decrease in the permeation rate of the PGE-2 and PGE-3  
25 membranes.

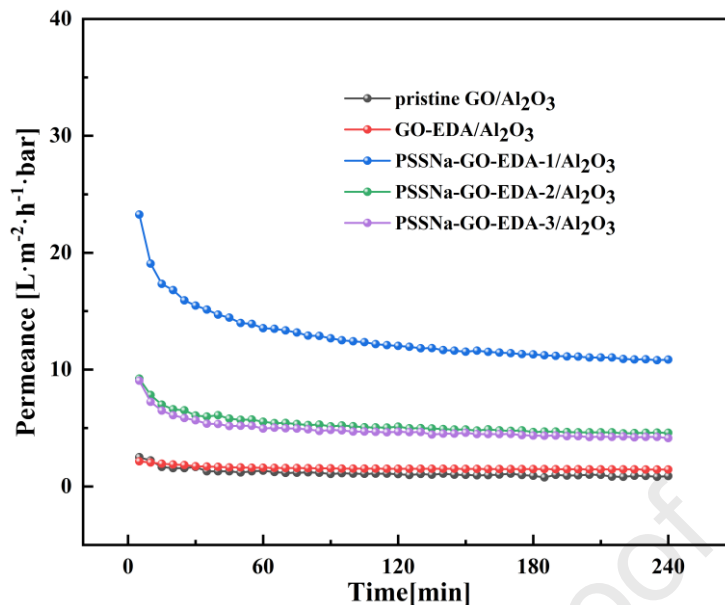


**Fig. 10.** Pure water permeance of pristine GO, GE, and PGE membranes

### 3.4 Desalination performance of GO-based membranes

To investigate the desalination performance of GO, GE, PGE-1, PGE- PGE-2, and PGE-3 membrane, the salt permeability and rejection were evaluated using four single-component salt solutions ( $\text{Na}_2\text{SO}_4$ ,  $\text{NaCl}$ ,  $\text{MgSO}_4$ ,  $\text{MgCl}_2$ ). Fig. 11 provides a visual representation of the results. The experimental results show that the rejection rates of the pristine GO membrane for  $\text{Na}_2\text{SO}_4$ ,  $\text{NaCl}$ ,  $\text{MgSO}_4$ , and  $\text{MgCl}_2$  are 79.8%, 47.0%, 72.7%, and 23.2%, respectively, indicating a varied performance for different solutes. This finding is in agreement with those of previous studies [2, 12]. After crosslinking of the EDA, a decrease in salt rejection was observed, which agrees with the previous report [39]. The rejection rates of GO and GE membranes for the four single-component salt solutions are ranked as follows:  $\text{Na}_2\text{SO}_4 > \text{MgSO}_4 > \text{NaCl} > \text{MgCl}_2$ , due to the synergistic effects of Donnan exclusion and size sieving[40].

In detail, based on the zeta potential results discussed above, GO and GE membranes are negatively charged. These membranes preferentially repel ions with the same charge as the GO membrane and attract ions with the opposite charge to the GO membrane, thereby ensuring the maintenance of charge neutrality throughout the entire system. This result can be attributed to the Donnan exclusion theory, as expressed in

1 Eq. (3):

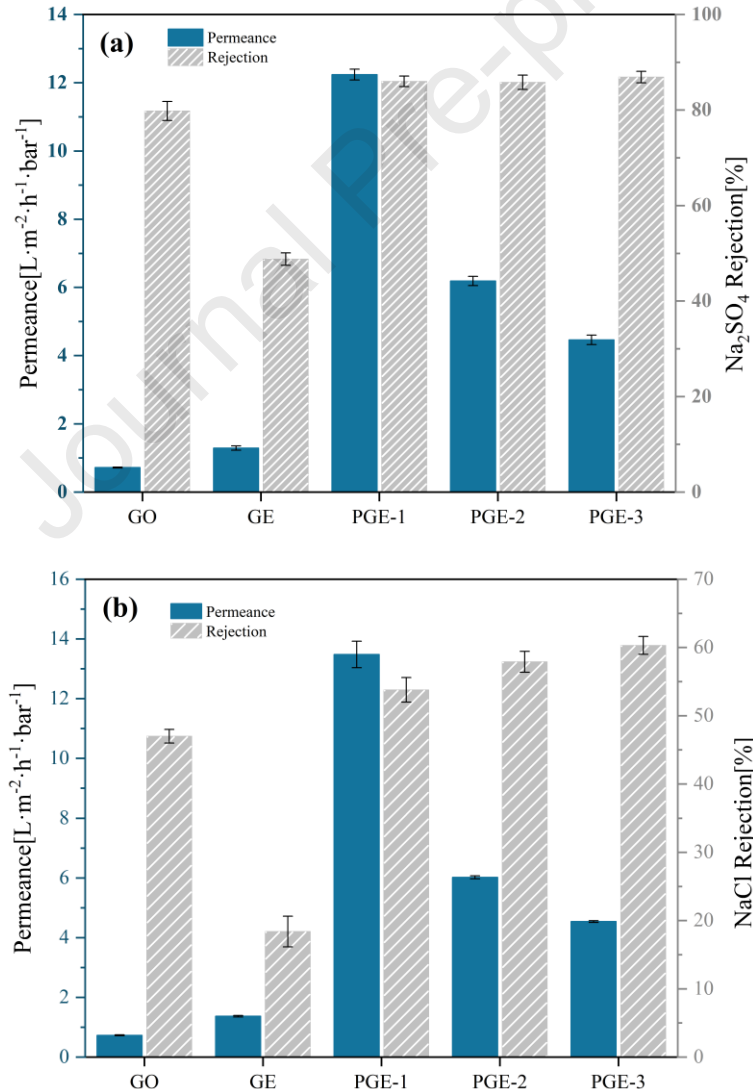
2

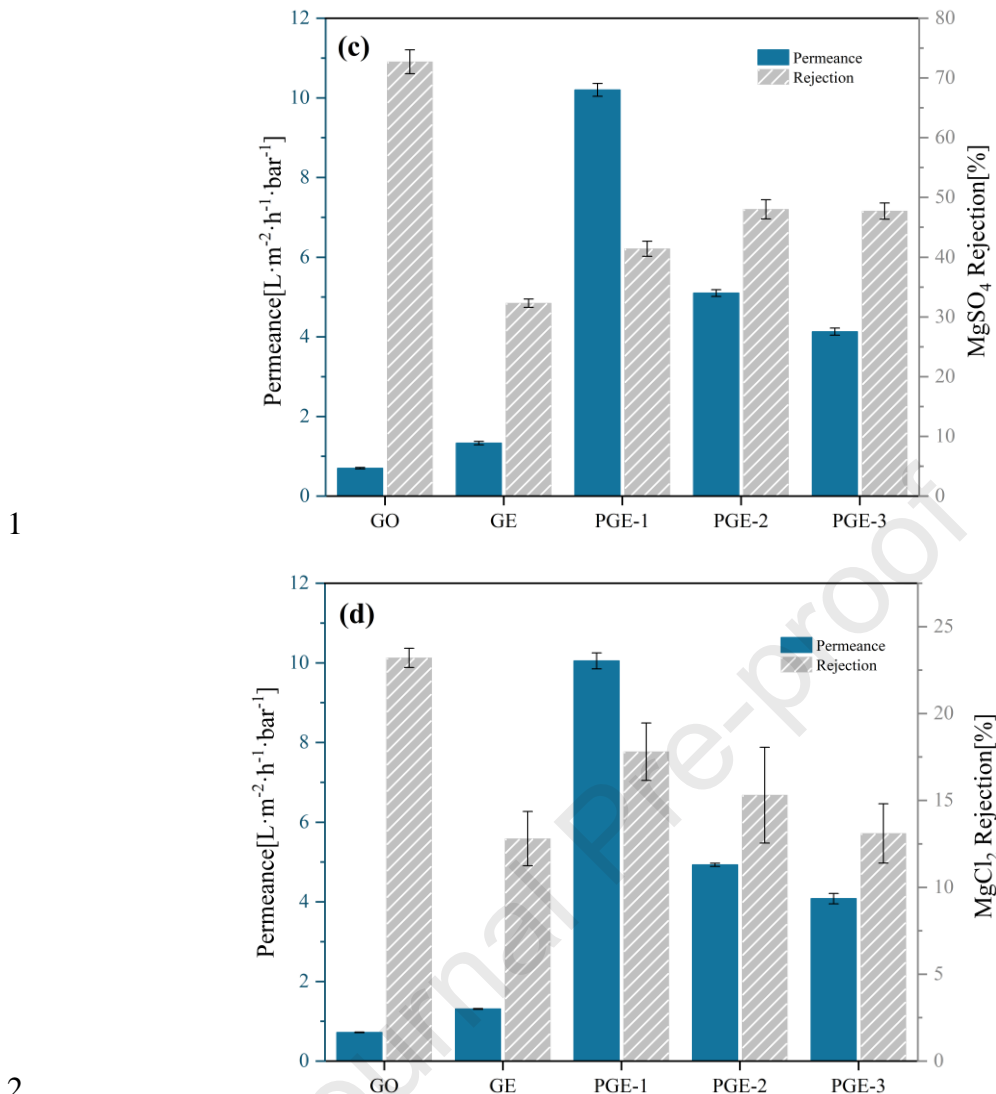
$$R = 1 - \frac{C_B^m}{C_B} = 1 - \left( \frac{|Z_B| C_B}{|Z_B| C_B + C_X^m} \right)^{|Z_B|/|Z_A|} \quad (3)$$

3 According to Eq. (3), the expected salt rejection order is  $R(\text{Na}_2\text{SO}_4) > R(\text{NaCl}) \approx$   
4  $R(\text{MgSO}_4) > R(\text{MgCl}_2)$ . However, experimental results indicated that the rejection of  
5  $\text{MgSO}_4$  exceeded that of  $\text{NaCl}$ . This result can be ascribed to the varying hydration  
6 diameters of the respective ions, as evidenced by the hydration diameters of the ions:  
7  $\text{Mg}^{2+}$  (8.6 Å) >  $\text{SO}_4^{2-}$  (7.6 Å) >  $\text{Na}^+$  >  $\text{Cl}^-$  (6.6 Å) [41]. Thus, the hydration diameters  
8 of  $\text{Mg}^{2+}$  and  $\text{SO}_4^{2-}$  are larger compared to those of  $\text{Na}^+$  and  $\text{Cl}^-$ , the latter of which are  
9 more readily rejected.

10

11





3 **Fig. 11.** Permeance and separation performance of GO and GE and PGE membranes  
4 towards four single-component salt solutions (a)  $Na_2SO_4$ , (b)  $NaCl$ , (c)  $MgSO_4$ , (d)  
5  $MgCl_2$

6 With regard to the PGE (PGE-1, PGE-2, PGE-3) membranes, the high permeability was  
7 sustained while a high salt rejection rate was also maintained, as shown in Fig. 11.  
8 Interestingly, the permeability of the salt solutions of the PGE membranes (PGE-1,  
9 PGE-2, PGE-3) was found to exceed that of the steady-state pure water of the PGE  
10 membranes (PGE-1, PGE-2, PGE-3). This was attributed to the fact that, during the  
11 testing of salt rejection, the permeate was collected immediately after stabilization for  
12 40 min. Based on the osmotic pressure formula proposed by van't Hoff, osmotic  
13 pressure is directly proportional to the molar concentration of solute in the solution [42].  
14 Salt solutions, which contain a high concentration of solutes, exhibit significantly

1 higher osmotic pressures compared to pure water. During nanofiltration, the osmotic  
 2 pressure of the solution generates a counteracting force opposing the driving force,  
 3 thereby impeding the permeation of water molecules from the feed side through the  
 4 membrane. In contrast, pure water, devoid of osmotic pressure, enables water molecules  
 5 to pass through the nanofiltration membrane more efficiently under identical operating  
 6 conditions, thus demonstrating superior permeability. Moreover, the viscosity of salt  
 7 solutions is generally greater than that of pure water, increasing flow resistance and  
 8 consequently resulting in lower permeability for salt solutions compared to pure water.  
 9 The relationship is given by Eq. (4):

10 
$$\Pi = icRT \quad (4)$$

11 Where  $\Pi$  (Pa) is the osmotic pressure;  $i$  is the van't Hoff factor;  $c$  ( $\text{mol}\cdot\text{m}^{-3}$ ) is the molar  
 12 concentration of the solute;  $R$  is the ideal gas constant,  $R=8.314\text{J}\cdot\text{mol}^{-1}\cdot\text{K}^{-1}$ ;  $T$  (K) is  
 13 the thermodynamic temperature.

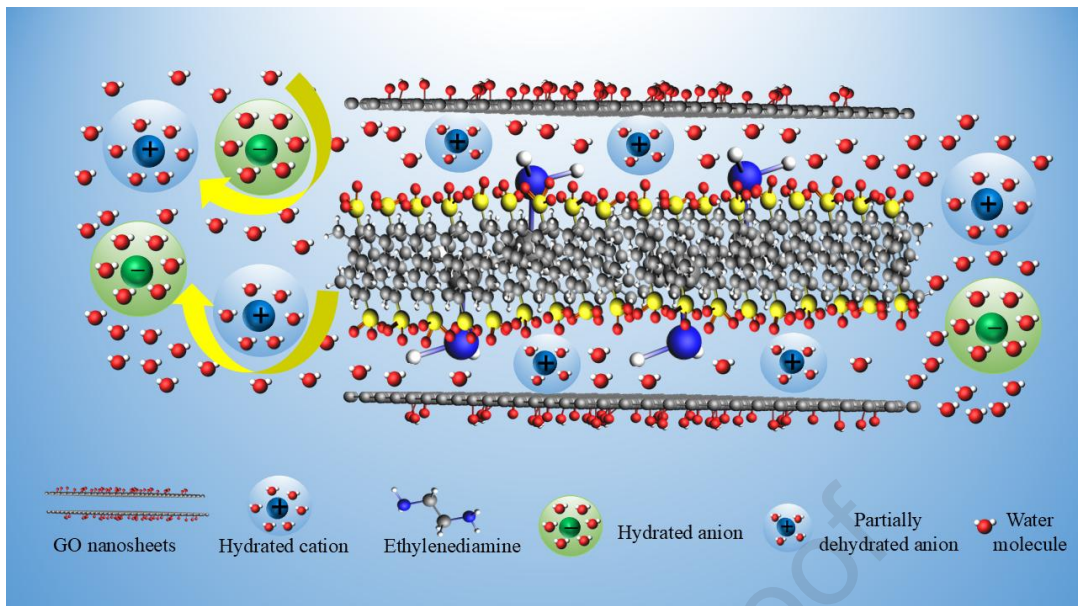
14 After the same stabilization time, the slightly lower salt solution permeance compared  
 15 to pure water permeance might be the consequence of higher osmotic pressure  
 16 difference across the membrane and higher viscosity in the salt solution [43]. In addition,  
 17 the rejection rates of PGE (PGE-1, PGE-2, PGE-3) membranes to  $\text{Na}_2\text{SO}_4$  were 86.0%,  
 18 85.8%, and 86.9%, and those to  $\text{NaCl}$  were 53.8%, 57.9%, and 60.3%, respectively,  
 19 which were all improved compared with those of GO and GE membranes.

20 Overall, the results demonstrate that PGE membranes (PGE-1, PGE-2, PGE-3)  
 21 exhibit superior water permeability compared to most GO-based membranes while  
 22 sustaining high salt rejection. This performance can primarily be attributed to two key  
 23 factors, as illustrated in Fig. 12.

24 When a salt ion traverses a separation membrane to maintain electrical neutrality  
 25 within the entire system, the salt ion is unable to permeate the membrane unassisted.  
 26 Instead, it must form an electrically neutral ion-pair (*i.e.*, in the form of a salt molecule)  
 27 with a counter-ion (also known as the equilibrium ion), which together with the pores  
 28 from the membrane, enables its permeation through the membrane. Similarly, ions

1 cannot be retained by the membrane alone; in order to ensure the electrical neutrality  
2 of the system, the ion must be retained by the membrane in an ion pair with its counter-  
3 ion (the equilibrium ion) [44, 45]. Moreover, the transport of individual ions through  
4 nanometer or sub-nanometer membrane pores has been shown to be controlled by the  
5 intra-pore diffusion of ions [45, 46], which is influenced by interactions between the  
6 ions and the pore wall [47]. These interactions, typically electrostatic in nature,  
7 encompass both attractive and repulsive forces between the fixed charges on the  
8 membrane surface and the ions [48]. This underlines the significance of ion-pore  
9 interactions and intra-pore cation/anion modulation.

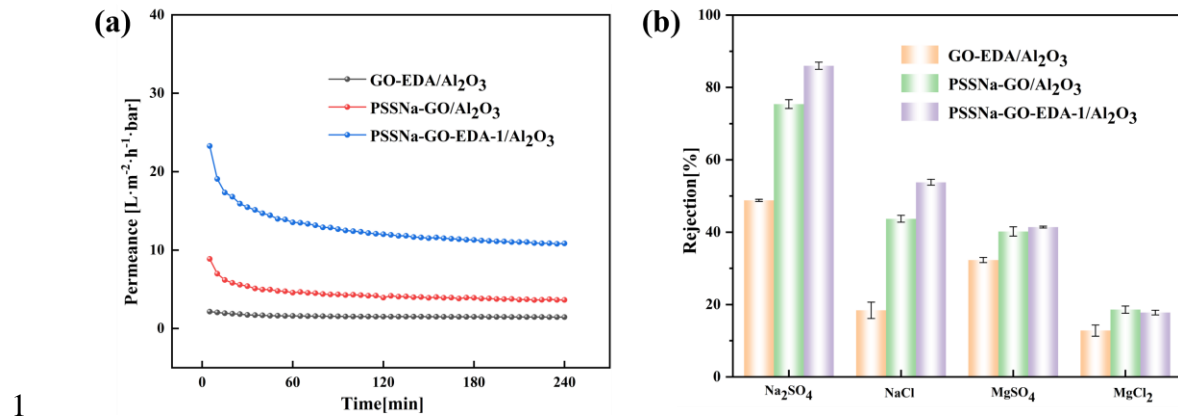
10 In contrast, the diffusion of ions in the lamellar channels of the PGE membrane is  
11 not only affected by the interactions of GO nanosheets on both sides of the nano-  
12 channels, but most importantly affected by the interactions between the ions and the  
13 PSSNa inserted in the interlayer. Consequently, the PGE membrane can achieve a high  
14 salt removal rate due to the introduction of poly(sodium 4-styrenesulfonate) polymer  
15 chains into the lamellar GO membrane, which leads to the formation of a hydrophilic  
16 nano-confined structure. The sulfonic groups within this structure then draw in ions  
17 through electrostatic induction, effectively confining them within the interlayer  
18 structure of the PGE membrane [49]. Thus, when salt ions traverse the membrane, they  
19 are affected by the aforementioned mechanism and are unable to pass through the  
20 membrane in the form of ion pairs with their equilibrium ions, thereby weakening their  
21 synergistic transport effect and achieving desalination. Additionally, the rejection of the  
22 PGE membranes to the four single-component salt solutions is also consistent with the  
23  $R(\text{Na}_2\text{SO}_4) > R(\text{NaCl}) > R(\text{MgSO}_4) > R(\text{MgCl}_2)$  order, which is in line with the Donnan  
24 effect theory. This indicates that the Donnan exclusion effect also contributes  
25 significantly



1 **Fig. 12.** Schematic illustration of separation mechanism through PGE membranes  
 2 nanochannel.  
 3

4 **3.5 Synergistic mechanism of EDA and PSSNa**

5 Figure 13 and Table 1 show the comparison of the nanofiltration performance  
 6 between GO-EDA, PSSNa-GO, and PSSNa-GO-EDA-1 membranes (GO:  
 7 PSSNa=1:150). It was observed that the nanofiltration performance of GO-EDA and  
 8 PSSNa-GO membranes was significantly inferior to that of PSSNa-GO-EDA-1  
 9 membranes. This suggests that the trade-off between selectivity and permeability can  
 10 effectively be overcome only when EDA and PSSNa are simultaneously intercalated  
 11 and crosslinked in GO membranes. The permeability of the membrane is enhanced by  
 12 an order of magnitude (12 times higher than that of pristine GO membranes), while  
 13 maintaining a high salt rejection rate. This improvement can be attributed to the  
 14 synergistic effect of EDA and PSSNa, which not only further enhances the stability of  
 15 GO membranes in water environments (Figure 9(c)), but also establishes hydrophilic  
 16 nanoconfined microregions between GO layers by leveraging the unique properties of  
 17 PSSNa. Such hydrophilic nanoconfined microregions facilitate the rapid and selective  
 18 transport of water molecules and meanwhile improve the rejection of charged ions by  
 19 GO membranes.



2 **Fig. 13.** Nanofiltration performance of GO-EDA, PSSNa-GO, PSSNa-GO-EDA-1  
3 membrane (a) Pure water permeance (b) rejection performance for four salt solutions

4  
5 **Table 1** Nanofiltration performance of GO-EDA, PSSNa-GO, and PSSNa-GO-EDA-  
6 1 membrane

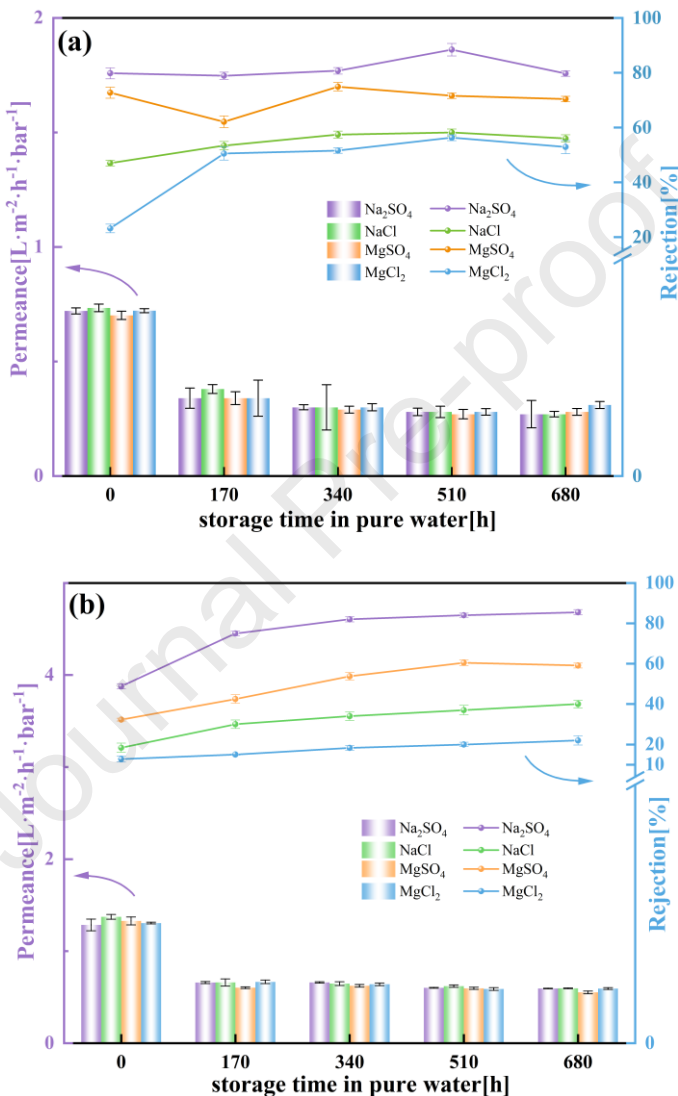
Membrane	<i>J</i> /	<i>R</i> /%			
	/LMH·bar <sup>-1</sup>	Na <sub>2</sub> SO <sub>4</sub>	NaCl	MgSO <sub>4</sub>	MgCl <sub>2</sub>
GO-EDA	1.46	48.8	18.4	32.3	12.8
PSSNa-GO-EDA-1	10.85	86.0	53.8	41.4	17.8
PSSNa-GO	3.65	75.4	43.7	40.2	18.6

### 7 3.6 Stability of GO-based membranes

8 The practical application of GO, GE, and PGE membranes is significantly  
9 hindered by their instability. Therefore, the application stability of the GO, GE, and  
10 PGE-1, PGE-2, PGE-3 membranes was tested by immersing them in pure water for  
11 varying periods of time. From Fig. 14, the permeance of the five GO-based membranes  
12 exhibits a slight decrease as the immersion time extends, whereas the rejection rates for  
13 the four salt solutions exhibit an increasing trend. After being immersed in water for  
14 680 hours, the rejection rates of GO, GE, PGE-1, PGE-2, PGE-3 membranes to Na<sub>2</sub>SO<sub>4</sub>  
15 reached 79.7%, 76.1%, 83.8%, 91.3% and 86.9%, respectively. The rejection rates of  
16 PGE membranes to four single-component salts exhibited minimal fluctuation within a

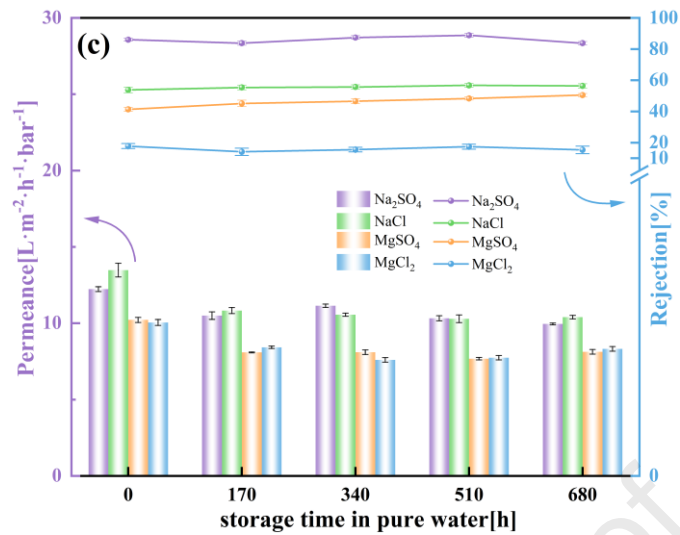
1 defined range and slight change with the prolongation of immersion time. This finding  
 2 indicates that the prepared membranes maintain remarkable stability in aqueous  
 3 solutions. The reason may lie in the fact that the residual cation ions between layers  
 4 produced cross-linking reactions with the GO nanosheets after many salt retention tests  
 5 [11], increasing the density of the membrane.

6

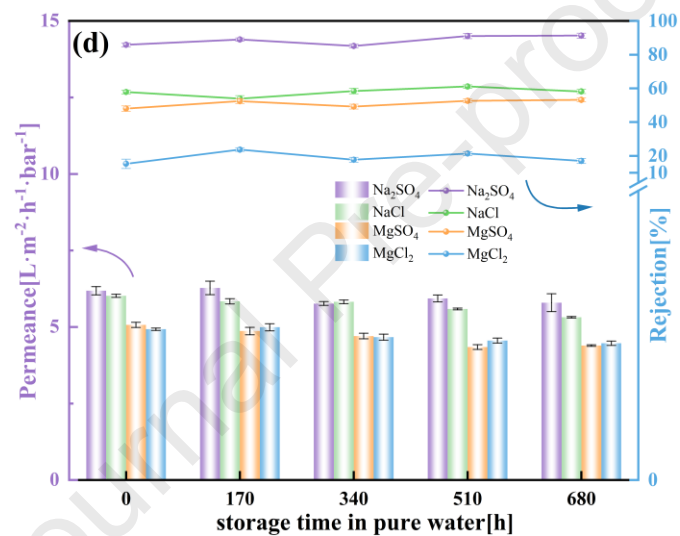


7

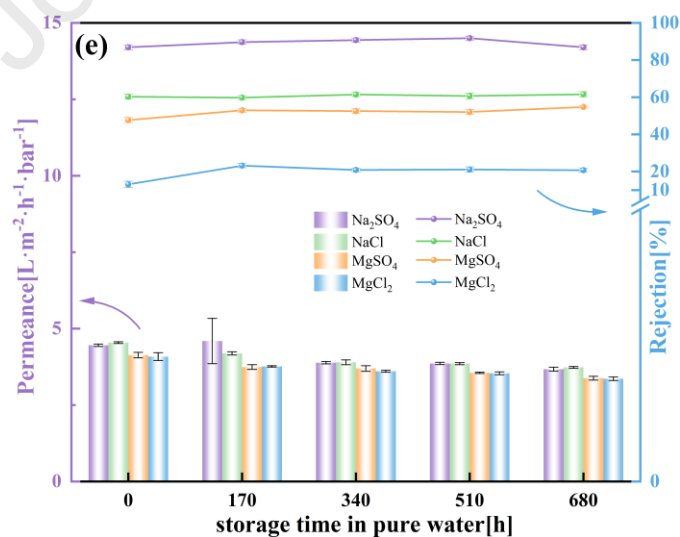
1



2



3



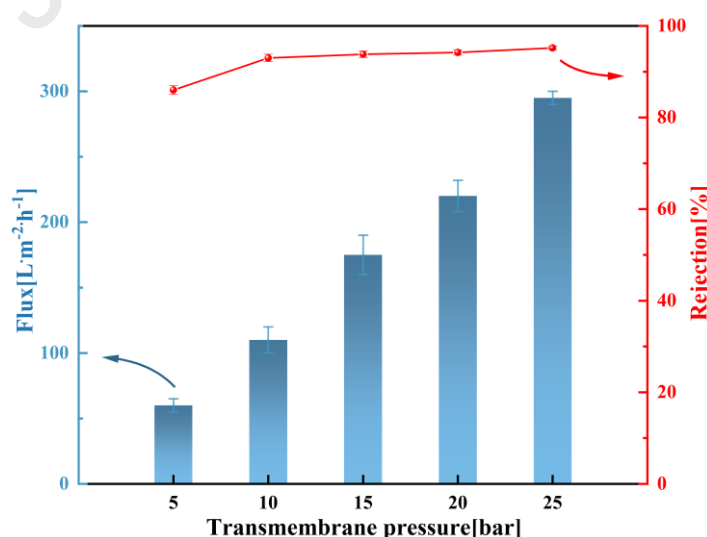
4

**Fig. 14.** Stability of GO and GE and PGE membranes (a) GO, (b) GE, (c) PGE-1, (d)

5

PGE-2, (e) PGE-3

1 The mechanical stability of PGE-1 membrane is essential in industrial separation  
 2 applications. Consequently, we also tested the mechanical stability of the PGE-1  
 3 membrane under higher operating pressure. With the escalation of the operating  
 4 pressure, the permeability of the PGE-1 membrane approximates a linear increase, and  
 5 the rejection rate of  $\text{Na}_2\text{SO}_4$  also shows an ascending tendency (as shown in Fig. 15.).  
 6 At 25 bar, the salt permeability reaches  $295 \text{ L}\cdot\text{m}^{-2}\cdot\text{h}^{-1}$ , with a  $\text{Na}_2\text{SO}_4$  rejection rate of  
 7 95.2%. Under high pressure, the PGE-1 lamellar membrane still exhibits outstanding  
 8 nanofiltration performance, thereby demonstrating its stable microstructure and high-  
 9 pressure resistance. Under high-pressure circumstances, the performance of the  
 10 membrane shows an upward trend. This trend can be analyzed by the dissolution-  
 11 diffusion theory [50]. The salt permeance is determined by the difference in salt  
 12 concentrations across the membrane. With the increase of pressure, the net pressure  
 13 difference across the membrane rises, intensifying the concentration polarization of the  
 14 membrane and consequently leading to elevated salt permeance. The salt rejection rate  
 15 is dependent upon the concentration of salt in the permeate. If the rate of salt permeation  
 16 exceeds that of water permeation, the salt rejection efficiency diminishes. Conversely,  
 17 when the water permeation rate surpasses that of salt permeation, the salt rejection  
 18 efficiency is enhanced.



19  
 20 **Fig. 15.** Rejection of PGE-1 membrane towards  $1 \text{ mmol}\cdot\text{L}^{-1}$   $\text{Na}_2\text{SO}_4$  solution under  
 21 5, 10, 15, 20, 25 bar

1       Compared with the GO nanofiltration membranes reported in previous reports, the  
 2       PGE-1 membrane in this paper still has highly competitive performance, as summarized  
 3       in Table 1.

4       **Table 2.** Comparison of performance for PGE-1 membrane with literature data for  
 5       other membranes.

Membrane	Support	Feed condition	Testing condition	Water permeance / $\text{LMH}\cdot\text{bar}^{-1}$	Rejection /%	Ref.
Pristine GO	$\alpha\text{-Al}_2\text{O}_3$	$\text{Na}_2\text{SO}_4, \text{MgSO}_4$ $\text{MgCl}_2, \text{NaCl}$	0.01% 5 bar	3.68	72.6, 58.4 23.7, 45.8	[12]
RGO	PVDF	$\text{Na}_2\text{SO}_4, \text{NaCl}$ $\text{MgSO}_4, \text{MgCl}_2$	$20 \text{ mmol}\cdot\text{L}^{-1}$ 5 bar	3.3	$\sim 60, \sim 30$ $\sim 20, \sim 40$	[51]
RGO/sGO	PVDF	$\text{Na}_2\text{SO}_4, \text{NaCl}$ $\text{MgSO}_4, \text{MgCl}_2$	$1 \text{ mmol}\cdot\text{L}^{-1}$ 2 bar	3.78	86.3, 60.5 40.9, 35.7	[52]
RGO/g-C <sub>3</sub> N <sub>4</sub>	MCE	$\text{Na}_2\text{SO}_4, \text{NaCl}$	$10 \text{ mmol}\cdot\text{L}^{-1}$ 1 bar	2.0	89.2, 67.5	[53]
GO-PEI	PAN	$\text{Na}_2\text{SO}_4, \text{MgCl}_2,$ $\text{NaCl}$	$10 \text{ mmol}\cdot\text{L}^{-1}$ 3 bar	4.0	30, 72 20	[54]
MoS <sub>2</sub> /GO	PVDF	$\text{Na}_2\text{SO}_4, \text{NaCl}$ $\text{MgSO}_4, \text{MgCl}_2$	$1 \text{ mmol}\cdot\text{L}^{-1}$ 2 bar	10.2	65.2, 43.2 24.3, 26.5	[55]
Commercial NF1	PS	$\text{Na}_2\text{SO}_4, \text{NaCl}$	/ 20 bar	3.45	98, 51	[56]
Commercial NF2	PAM	$\text{Na}_2\text{SO}_4, \text{NaCl}$	/ 20 bar	6.5	99, 44	[56]
Osmonics DK	/	NaCl	$\text{g}\cdot\text{L}^{-1}$ /	3.05	22.0~75.6	[57]
Osmonics CK	/	NaCl	$0.059\text{--}5.85$ $\text{g}\cdot\text{L}^{-1}$ /	2.42	45.5~77.7	[57]
PGE-1	$\text{Al}_2\text{O}_3$	$\text{Na}_2\text{SO}_4, \text{NaCl}$	$1 \text{ mmol}\cdot\text{L}^{-1}$ 5 bar	10.85	86.0, 53.8	This work

#### 6       4. Conclusion

7       In this paper, PSSNa-GO-EDA/ $\text{Al}_2\text{O}_3$  membranes were successfully prepared by  
 8       embedding PSSNa into amine-crosslinked GO interlayers using a pressure-driven  
 9       deposition technique on tubular  $\text{Al}_2\text{O}_3$  ultrafiltration membranes. The introduction of  
 10      hydrophilic PSSNa polymer chains between GO interlayers not only enhances the

1 regulation of interlayer spacing but also improves the chemical microenvironment. The  
 2 introduced sulfonic acid groups significantly augment the hydrophilicity of the  
 3 membrane, enhance its selective transportation of water molecules, and greatly boost  
 4 its permeability. Furthermore, a nanoconfinement structure was fabricated in the  
 5 laminar GO membranes by long-chain polystyrene sulfonic acid, which confines ions  
 6 within the interlayer channels via the electrostatic attraction between sulfonic acid  
 7 groups and ions. This breaks the correlation of anions and cations to suppress anion-  
 8 cation co-transport, substantially improving the nanofiltration performance of the GO-  
 9 based membranes. Of the GO, GE, and PGE membranes, the PGE-1 membrane  
 10 maintains high salt rejection rates and increases water permeability by more than  
 11 tenfold, and thus it demonstrates excellent separation performance and desalination  
 12 stability. It also maintains favorable long-term stability, retaining high desalination  
 13 performance even after being immersed in pure water for 680 hours. In conclusion, the  
 14 construction of specialized domain-confined structures and targeted chemical  
 15 microenvironments between the 2D membrane interlayers could be an effective  
 16 strategy for achieving the ultrahigh nanofiltration performance of GO-based  
 17 membranes and for applying them to real systems.

## 18 **Acknowledgments**

19 This study was supported by the National Natural Science Foundation of China  
 20 (21490581) and China Petroleum & Chemical Corporation (317008-6).

## 21 **References:**

- 22 [1] P.J.J. Alvarez, C.K. Chan, M. Elimelech, N.J. Halas, D. Villagrán, Emerging opportunities  
 23 for nanotechnology to enhance water security, *Nat. Nanotechnol.* 13 (8) (2018) 634–641.
- 24 [2] Y.Y. Wu, C.F. Fu, Q. Huang, P.P. Zhang, P. Cui, J. Ran, J.L. Yang, T.W. Xu, 2D  
 25 heterostructured nanofluidic channels for enhanced desalination performance of graphene  
 26 oxide membranes, *ACS Nano* 15 (4) (2021) 7586–7595.
- 27 [3] R.P. Lively, D.S. Sholl, From water to organics in membrane separations, *Nat. Mater.* 16 (3)  
 28 (2017) 276–279.
- 29 [4] B. Sapkota, W.T. Liang, A. VahidMohammadi, R. Karnik, A. Noy, M. Wanunu, High  
 30 permeability sub-nanometre sieve composite MoS<sub>2</sub> membranes, *Nat. Commun.* 11 (1) (2020)  
 31 2747.

1 [5] D.S. Sholl, R.P. Lively, Seven chemical separations to change the world, *Nature* 532 (7600) 2 (2016) 435–437.

3 [6] J. Shen, G.P. Liu, Y. Han, W.Q. Jin, Artificial channels for confined mass transport at the 4 sub-nanometre scale, *Nat. Rev. Mater.* 6 (2021) 294–312.

5 [7] Z.D. Xiong, L.H. Dai, Y.X. Wang, K. Qu, Y.S. Xia, L.F. Lei, K. Huang, Z. Xu, Two- 6 dimensional sub-nanometer confinement channels enabled by functional carbon dots for ultra- 7 permeable alcohol dehydration, *J. Membr. Sci.* 644 (2022) 120069.

8 [8] L.Y. Zhang, M.C. Zhang, G.P. Liu, W.Q. Jin, X.Y. Li, Fungal cell wall-graphene oxide 9 microcomposite membrane for organic solvent nanofiltration, *Adv. Funct. Mater.* 31 (23) (2021) 10 2100110.

11 [9] W.H. Zhang, M.J. Yin, Q. Zhao, C.G. Jin, N.X. Wang, S.L. Ji, C.L. Ritt, M. Elimelech, Q.F. 12 An, Graphene oxide membranes with stable porous structure for ultrafast water transport, *Nat. 13 Nanotechnol.* 16 (3) (2021) 337–343.

14 [10] G. Romanos, L.M. Pastrana-Martínez, T. Tsoufis, C. Athanasekou, E. Galata, F. Katsaros, 15 E. Favvas, K.G. Beltsios, E. Siranidi, P. Falaras, V. Psycharis, A.M.T. Silva, A facile approach 16 for the development of fine-tuned self-standing graphene oxide membranes and their gas and 17 vapor separation performance, *J. Membr. Sci.* 493 (2015) 734–747.

18 [11] C.N. Yeh, K. Raidongia, J.J. Shao, Q.H. Yang, J.X. Huang, On the origin of the stability of 19 graphene oxide membranes in water, *Nat. Chem.* 7 (2) (2014) 166–170.

20 [12] B.Q. Yuan, M.X. Wang, B. Wang, F.L. Yang, X. Quan, C.Y. Tang, Y.C. Dong, Cross-linked 21 graphene oxide framework membranes with robust nano-channels for enhanced sieving ability, 22 *Environ. Sci. Technol.* 54 (23) (2020) 15442–15453.

23 [13] S. Wang, S.S. Liang, L. Chen, H.P. Fang, Realizing ultrahigh nanofiltration performance 24 based on small flake reduced graphene oxide membranes, *Desalination* 528 (2022) 115601.

25 [14] S.X. Zheng, Q.S. Tu, J.J. Urban, S.F. Li, B.X. Mi, Swelling of graphene oxide membranes 26 in aqueous solution: characterization of interlayer spacing and insight into water transport 27 mechanisms, *ACS Nano* 11 (6) (2017) 6440–6450.

28 [15] P.C. Su, F. Wang, Z.J. Li, C.Y. Tang, W.B. Li, Graphene oxide membranes: controlling 29 their transport pathways, *J. Mater. Chem. A* 8 (31) (2020) 15319–15340.

30 [16] J. Wang, H.J. Zhou, S.Z. Li, L. Wang, Selective ion transport in two-dimensional lamellar 31 nanochannel membranes, *Angew. Chem. Int. Ed.* 62 (19) (2023) e202218321.

32 [17] J. Abraham, K.S. Vasu, C.D. Williams, K. Gopinadhan, Y. Su, C.T. Cherian, J. Dix, E. 33 Prestat, S.J. Haigh, I.V. Grigorieva, P. Carbone, A.K. Geim, R.R. Nair, Tunable sieving of ions 34 using graphene oxide membranes, *Nat. Nanotechnol.* 12 (6) (2017) 546–550.

35 [18] N.K. Khanzada, S. Rehman, S.Y. Leu, A.K. An, Evaluation of anti-bacterial adhesion 36 performance of polydopamine cross-linked graphene oxide RO membrane *via in situ* optical 37 coherence tomography, *Desalination* 479 (2020) 114339.

38 [19] S. Rajesh, A.B. Bose, Development of graphene oxide framework membranes *via* the 39 “from” and “to” cross-linking approach for ion-selective separations, *ACS Appl. Mater. 40 Interfaces* 11 (31) (2019) 27706–27716.

41 [20] I. Chandio, F.A. Janjhi, A. Ali Memon, S. Memon, Z. Ali, K.H. Thebo, A. Ali Ayaz Pirzado, 42 A. Ali Hakro, W.S. Khan, Ultrafast ionic and molecular sieving through graphene oxide based

1 composite membranes, *Desalination* 500 (2021) 114848.

2 [21] F. Ahmed Janjhi, I. Chandio, A. Ali Memon, Z. Ahmed, K. Hussain Thebo, A. Ali Ayaz  
3 Pirzado, A. Ali Hakro, M. Iqbal, Functionalized graphene oxide based membranes for ultrafast  
4 molecular separation, *Sep. Purif. Technol.* 274 (2021) 117969.

5 [22] E. Halakoo, X.S. Feng, Layer-by-layer assembled membranes from graphene oxide and  
6 polyethyleneimine for ethanol and isopropanol dehydration, *Chem. Eng. Sci.* 216 (2020)  
7 115488.

8 [23] D. Mengchen Zhang, Y.Y. Mao, G.Z. Liu, P. Gongping Liu, P. Yiqun Fan, P. Wanqin Jin,  
9 Molecular bridges stabilize graphene oxide membranes in water, *Angew. Chem. Int. Ed.* 59 (4)  
10 (2020) 1689–1695.

11 [24] F.C. Jia, L. Yang, Z.H. Li, L.Y. Sun, D.H. Yu, Y. Song, Y.X. Wang, L.J. Huang, J.G. Tang,  
12 Graphene oxide/sodium alginate nanofiltration membrane with double cross-linked structure  
13 for high-performance in dye separation, *J. Mater. Sci.* 58 (15) (2023) 6618–6631.

14 [25] J. Yu, Y. He, Y.Q. Wang, S.S. Li, S.T. Tian, Ethylenediamine-oxidized sodium alginate  
15 hydrogel cross-linked graphene oxide nanofiltration membrane with self-healing property for  
16 efficient dye separation, *J. Membr. Sci.* 670 (2023) 121366.

17 [26] D.L. Xu, H. Liang, X.W. Zhu, L. Yang, X.S. Luo, Y.Q. Guo, Y.T. Liu, L.M. Bai, G.B. Li,  
18 X.B. Tang, Metal-polyphenol dual crosslinked graphene oxide membrane for desalination of  
19 textile wastewater, *Desalination* 487 (2020) 114503.

20 [27] L.P. Shao, Y. Li, F.S. Pan, Z.M. Zhang, S.W. Liang, Y.T. Wang, J.Y. Zou, Z.Y. Jiang,  
21 Graphene oxide membranes tuned by metal-phytic acid coordination complex for butanol  
22 dehydration, *J. Membr. Sci.* 638 (2021) 119736.

23 [28] L.H. Dai, Z.D. Xiong, W.Y. Xu, K. Qu, Y.X. Wang, S.Y. Gu, H.Y. Cao, Y. Yu, L.F. Lei, S.Y.  
24 Li, K. Huang, X.H. Guo, Z. Xu, Two-dimensional confined channels with high-density  
25 hydrophilic microregions for enhanced selective water transport, *J. Membr. Sci.* 671 (2023)  
26 121398.

27 [29] R.Q. Cao, S.Y. Shi, H.B. Cao, Y.J. Li, F. Duan, Y.P. Li, Surface composite modification of  
28 anion exchange membrane by electrodeposition and self-polymerization for improved  
29 antifouling performance, *Colloids Surf. A Physicochem. Eng. Aspects* 648 (2022) 129402.

30 [30] K. Zahri, K.C. Wong, P.S. Goh, A.F. Ismail, Graphene oxide/polysulfone hollow fiber  
31 mixed matrix membranes for gas separation, *RSC Adv.* 6 (92) (2016) 89130–89139.

32 [31] S.J. Xia, M.Z. Ni, T.R. Zhu, Y. Zhao, N.N. Li, Ultrathin graphene oxide nanosheet  
33 membranes with various d-spacing assembled using the pressure-assisted filtration method for  
34 removing natural organic matter, *Desalination* 371 (2015) 78–87.

35 [32] Y.L. Qian, X.L. Zhang, C.Y. Liu, C. Zhou, A.S. Huang, Tuning interlayer spacing of  
36 graphene oxide membranes with enhanced desalination performance, *Desalination* 460 (2019)  
37 56–63.

38 [33] W.S. Hung, C.H. Tsou, M. De Guzman, Q.F. An, Y.L. Liu, Y.M. Zhang, C.C. Hu, K.R. Lee,  
39 J.Y. Lai, Cross-linking with diamine monomers to prepare composite graphene oxide-  
40 framework membranes with varying d-spacing, *Chem. Mater.* 26 (9) (2014) 2983–2990.

41 [34] Z. Lu, Y. Wu, L. Ding, Y.Y. Wei, H.H. Wang, A lamellar MXene ( $Ti_3C_2t_x$ )/PSS composite  
42 membrane for fast and selective lithium-ion separation, *Angew. Chem. Int. Ed* 60 (41) (2021)

1 22265–22269.

2 [35] F. Liang, H.Y. Wang, G.Z. Liu, J. Zhao, W.Q. Jin, Designing highly selective and stable  
3 water transport channel through graphene oxide membranes functionalized with polyhedral  
4 oligomeric silsesquioxane for ethanol dehydration, *J. Membr. Sci.* 638 (2021) 119675.

5 [36] S. Liu, G.Y. Zhou, K.C. Guan, X. Chen, Z.Y. Chu, G.P. Liu, W.Q. Jin, Dehydration of C2–  
6 C4 alcohol/water mixtures *via* electrostatically enhanced graphene oxide laminar membranes,  
7 *AIChE J.* 67 (6) (2021) aic17170.

8 [37] K.H. Thebo, X.T. Qian, Q. Zhang, L. Chen, H.M. Cheng, W.C. Ren, Highly stable  
9 graphene-oxide-based membranes with superior permeability, *Nat. Commun.* 9 (2018) 1486.

10 [38] J.Y. Chong, B. Wang, K. Li, Water transport through graphene oxide membranes: the roles  
11 of driving forces, *Chem. Commun.* 54 (20) (2018) 2554–2557.

12 [39] Y. Zhang, S. Zhang, T.S. Chung, Nanometric graphene oxide framework membranes with  
13 enhanced heavy metal removal *via* nanofiltration, *Environ. Sci. Technol.* 49 (16) (2015) 10235–  
14 10242.

15 [40] S.F. Wang, L.X. Yang, G.W. He, B.B. Shi, Y.F. Li, H. Wu, R.N. Zhang, S. Nunes, Z.Y.  
16 Jiang, Two-dimensional nanochannel membranes for molecular and ionic separations, *Chem.  
17 Soc. Rev.* 49 (4) (2020) 1071–1089.

18 [41] I. Shefer, O. Peer-Haim, R. Epsztein, Limited ion-ion selectivity of salt-rejecting  
19 membranes due to enthalpy-entropy compensation, *Desalination* 541 (2022) 116041.

20 [42] J.H. van't Hoff, The role of osmotic pressure in the analogy between solutions and gases,  
21 *J. Membr. Sci.* 100 (1) (1995) 39–44.

22 [43] M.C. Zhang, J.J. Sun, Y.Y. Mao, G.P. Liu, W.Q. Jin, Effect of substrate on formation and  
23 nanofiltration performance of graphene oxide membranes, *J. Membr. Sci.* 574 (2019) 196–204.

24 [44] I.V. Khavrutskii, A.A. Gorfe, B.Z. Lu, J. Andrew McCammon, Free energy for the  
25 permeation of Na(+) and Cl (-) ions and their ion-pair through a zwitterionic dimyristoyl  
26 phosphatidylcholine lipid bilayer by umbrella integration with harmonic Fourier beads, *J. Am.  
27 Chem. Soc.* 131 (5) (2009) 1706–1716.

28 [45] X. Zhou, Z. Wang, R. Epsztein, C. Zhan, W. Li, J.D. Fortner, T.A. Pham, J.H. Kim, M.  
29 Elimelech, Intrapore energy barriers govern ion transport and selectivity of desalination  
30 membranes, *Sci. Adv.* 6 (48) (2020) eabd9045.

31 [46] S.B. Sigurdardottir, R.M. DuChanois, R. Epsztein, M. Pinelo, M. Elimelech, Energy  
32 barriers to anion transport in polyelectrolyte multilayer nanofiltration membranes: Role of  
33 intra-pore diffusion, *J. Membr. Sci.* 603 (2020) 117921.

34 [47] R. Epsztein, R.M. DuChanois, C.L. Ritt, A. Noy, M. Elimelech, Towards single-species  
35 selectivity of membranes with subnanometre pores, *Nat. Nanotechnol.* 15 (2020) 426–436.

36 [48] C. Lu, C. Hu, Z. Chen, P. Wang, F. Feng, G. He, F. Wang, Y. Zhang, J.Z. Liu, X. Zhang, J.  
37 Qu, Dehydration-enhanced ion-pore interactions dominate anion transport and selectivity in  
38 nanochannels, *Sci. Adv.* 9 (27) (2023) eadf8412.

39 [49] H.G. Zhang, J.J. Xing, G.L. Wei, X. Wang, S. Chen, X. Quan, Electrostatic-induced ion-  
40 confined partitioning in graphene nanolaminate membrane for breaking anion-cation co-  
41 transport to enhance desalination, *Nat. Commun.* 15 (1) (2024) 4324.

42 [50] K. Popper, R.L. Merson, W.M. Camirand, Desalination by osmosis: reverse osmosis

1 couple, *Science* 159 (3821) (1968) 1364–1365.

2 [51] Y. Han, Z. Xu, C. Gao, Ultrathin graphene nanofiltration membrane for water purification,  
3 *Adv. Funct. Mater.* 23 (29) (2013) 3693–3700.

4 [52] P. Zhang, J.L. Gong, G.M. Zeng, B. Song, S.Y. Fang, M. Zhang, H.Y. Liu, S.Y. Huan, P.  
5 Peng, Q.Y. Niu, D.B. Wang, J. Ye, Enhanced permeability of rGO/S-GO layered membranes  
6 with tunable inter-structure for effective rejection of salts and dyes, *Sep. Purif. Technol.* 220  
7 (2019) 309–319.

8 [53] Z.J. Li, Y.C. Xing, X.Y. Fan, L.G. Lin, A.L. Meng, Q.D. Li, rGO/protonated g-C<sub>3</sub>N<sub>4</sub> hybrid  
9 membranes fabricated by photocatalytic reduction for the enhanced water desalination,  
10 *Desalination* 443 (2018) 130–136.

11 [54] Y. Liu, S.X. Zheng, P. Gu, A.J. Ng, M.N. Wang, Y.Y. Wei, J.J. Urban, B.X. Mi, Graphene-  
12 polyelectrolyte multilayer membranes with tunable structure and internal charge, *Carbon* 160  
13 (2020) 219–227.

14 [55] P. Zhang, J.L. Gong, G.M. Zeng, B. Song, W.C. Cao, H.Y. Liu, S.Y. Huan, P. Peng, Novel  
15 “loose” GO/MoS<sub>2</sub> composites membranes with enhanced permeability for effective salts and  
16 dyes rejection at low pressure, *J. Membr. Sci.* 574 (2019) 112–123.

17 [56] N.K. Zaman, R. Rohani, A.W. Mohammad, J.M. Jahim, New polymeric membrane  
18 nanofiltration for succinate recovery: a comparative study, *J. Polym. Res.* 24 (11) (2017) 197.

19 [57] A.W. Mohammad, R.K. Basha, C.P. Leo, Nanofiltration of glucose solution containing  
20 salts: Effects of membrane characteristics, organic component and salts on retention, *J. Food  
Eng.* 97 (4) (2010) 510–518.

22

23

## **Declaration of Competing Interest**

The authors declare that they have no known competing financial interests or personal relationships that could have appeared to influence the work reported in this paper.